PROCEEDINGS OF SPIE

SPIEDigitalLibrary.org/conference-proceedings-of-spie

Thermal diffusion effects in the spatial resolution of photothermal microscopy

Brendan Brown, Gregory Hartland

Brendan S. Brown, Gregory V. Hartland, "Thermal diffusion effects in the spatial resolution of photothermal microscopy," Proc. SPIE 11990, Nanoscale and Quantum Materials: From Synthesis and Laser Processing to Applications 2022, 1199007 (4 March 2022); doi: 10.1117/12.2607795



Event: SPIE LASE, 2022, San Francisco, California, United States

Thermal Diffusion Effects in the Spatial Resolution of Photothermal Microscopy

Brendan S. Brown*a, Gregory V. Hartland*a

^aDepartment of Chemistry and Biochemistry, University of Notre Dame, Notre Dame, IN 46556,USA

ABSTRACT

Photothermal microscopy is a powerful method for investigating biological systems and solid state materials. Using a modulated pump to excite the sample, a continuous probe beam monitors the change in the refractive index of the sample due to the modulated heating. These experiments are typically performed at high frequencies to reduce the 1/f noise, achieving a higher signal to noise ratio. In this paper, we explore how the resolution and sensitivity of the photothermal experiments change when the modulation frequency is brought down below 100kHz. In the instance that the pump and probe are cofocused at the sample, the resolution is determined by the size of the pump beam. On the other hand, when a widefield pump is used, significant broadening occurs for frequencies under 20kHz. This broadening is attributed to thermal diffusion. However, the amount of broadening is less than that expected from the thermal diffusion length, which is about 1.7µm at 10kHz for nanoparticles in glycerol. We also explore the situation where the point spread functions of the pump and probe beams are smaller than the particle size as well as how the penetration depth depends on the properties of the pump and probe beams.

Keywords: Photothermal Imaging, Thermal Diffusion, Spatial Resolution

1. INTRODUCTION

Photothermal Heterodyne Imaging (PHI) is a powerful technique for studying nanomaterials. ¹⁻³ The capacity of this technique includes detecting small metal and semiconductor nanoparticles, ² as well as single molecules. ⁴ Recently PHI has been expanded to create a super resolution infrared imaging technique (IR-PHI). ⁵⁻⁶ In PHI a modulated pump beam is used to induce heating of the sample through absorption. The heat is dissipated into the medium surrounding the sample, which creates a temperature gradient, also known as a thermal lens. ^{3,7-9} Traditionally for visible PHI, a thermal medium like glycerol is used in order to enhance the created thermal lens. The thermal lens is detected using a second non-resonant probe beam that is scattered by the lens. ^{3,7-9} In theory, the size of the thermal lens is dependent upon the thermal radius $R_{th} = (2\kappa/\omega C)^{1/2}$ where κ is the thermal conductivity, κ is the specific heat capacity and κ is the modulation frequency. ¹⁰ Because of the frequency dependence for the thermal radius, an interesting question is whether the spatial resolution in PHI is also frequency dependent.

Typically PHI experiments are performed at frequencies above 100 kHz in order to reduce 1/f noise in the experiments. At these frequencies, R_{th} is less than the size of a focused beam. In order to look at the frequency dependence, frequencies under 50 kHz were needed, which have not been extensively examined due to the rising 1/f noise. It's at these low frequencies that R_{th} becomes larger than a diffraction limited beam, making it an interesting region to investigate resolution in PHI images. In addition, especially in the case of IR-PHI, there can be limitations in the modulation frequency for the pump beam in PHI experiments, ounderstanding the frequency dependence of spatial resolution is a significant issue.

*Further author information: (send correspondence to B.S.B. or G.V.H.)

B.S.B.: E-mail: bbrown13@nd.edu G.V.H.: E-mail: ghartlan@nd.edu

Nanoscale and Quantum Materials: From Synthesis and Laser Processing to Applications 2022, edited by Andrei V. Kabashin, Maria Farsari, Masoud Mahjouri-Samani, Proc. of SPIE Vol. 11990, 1199007 · © 2022 SPIE · 0277-786X · doi: 10.1117/12.2607795

In this study the spatial resolution of PHI was explored using both experiments as well as finite element simulations of heat diffusion. Experimentally, gold nanoparticles on glass coated with glycerol were imaged at different pump modulation frequencies using both co-focused pump and probe beams, as well as a widefield pump with a focused probe. Heat transfer simulations were used to study the thermal decay for gold nanoparticles in a homogeneous environment of glycerol. The simulations provide information about the temperature profile around the gold nanoparticle and allow us to understand the experimental results.

2. METHODS

2.1 PHI measurements.

Measurements were performed using a homebuilt microscope. The pump beam was a 532nm beam produced by a Spectra-Physics Millenia Vs and was fed through an acousto-optic modulator (AOM) to produce a square wave modulated pump. The AOM was driven by either an SR830 or SR844 lock-in amplifier, depending on the frequency (the SR844 was used for frequencies above 100 kHz). The probe beam was a 636nm Coherent Obis. Both the beams were passed through spatial filters to improve beam quality before being coaligned using a dichroic mirror. The two beams were focused onto the sample by a Nikon Plan Apo 40x/0.95 NA air objective and collected in transmission by an Olympus UPlanFl 10x/0.30 NA air objective. Optical filters were used to extinguish the pump beam, and the collected probe was then focused onto an amplified photodetector with the gain setting set to 10x. The measurements were performed in transmission since a better signal-to noise was achieved. In order to create a widefield pump, a 250 mm focal length lens was placed in the pump beam path before the dichroic mirror.

2.2 Sample preparation

50nm gold nanoparticles purchased from nanoComposix (product number AUCN50) were used for the experiments. A plasma cleaned bk7 #1.5 coverslip had $200~\mu L$ of stock gold solution drop cast onto it. The solution was allowed to rest for 10 minutes, then any excess liquid was removed by wicking with a paper towel. A drop of glycerol was then added to the sample, and a second plasma cleaned coverslip was placed on top to ensure a uniform environment for transmission measurements.

2.3 Finite Element Simulations

COMSOL Multiphysics (v.5.3) was used to perform finite element simulations of heat transfer for gold nanoparticles into their environments. Gold nanoparticles were modeled as a sphere with a radius of 25nm, with the environment being modeled as a sphere with $4\mu m$ radius. The initial temperature of the whole system was 300K, and the outer surface of the environment was set to 300K as a boundary condition. A square wave source was used to heat the gold nanoparticle, modeled after the heating used in the experiments, with the power adjusted to give a maximum temperature of about 310K. The simulations were performed at a range of frequencies to observe how the temperature profile around the gold nanoparticle acted as a function of frequency.

3. RESULTS AND DISCUSSION

The first set of experiments performed were for co-focused pump and probe beams at different modulation frequencies. These are akin to the traditional setup of PHI where the beams are focused by the same objective and therefore are on the same order of magnitude in size (using visible/near-infrared pump and probes). A longer time constant was needed for the 1 kHz scan due to the aforementioned 1/f noise problem. Figure 1 shows that there was no change in resolution due to frequency. At 100 kHz the thermal radius is $0.52~\mu m$ and it broadens out to $5.2~\mu m$ at 1 kHz. Which means that if the experiment was to follow the thermal radius as predicted, the image for 1 kHz should be at least 4x larger in size. Thus, the spatial resolution does not change as the frequency is changed. This is attributed to the fact that there is no thermal lens when the pump beam is off the particle, since the particle is not being heated. Thus the spatial resolution for a co-focused pump and probe beam PHI setup is determined by the size of the pump beam at focus.

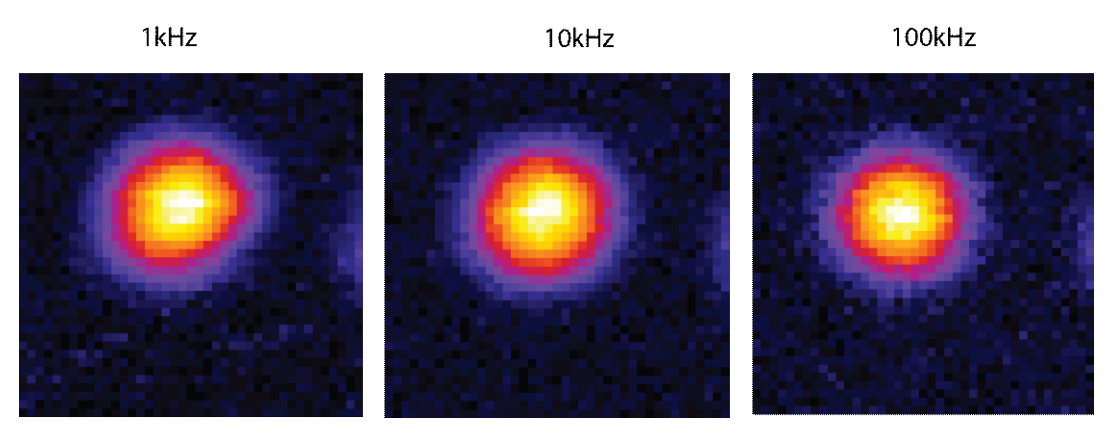


Figure 1. PHI image of a 50 nm gold nanoparticle using co-focused pump and probe beams. The scan area was $2x2 \mu m$ with a step size of 50 nm. The modulation frequency for each image is shown at the top. For the 10 and 100 kHz images the time constant used was 10 ms, and for the 1 kHz the time constant used was 100ms.

In order to fully examine whether or not there is a frequency dependence, a widefield pump was used instead of a focused pump. By making the pump size about $80 \mu m$, done by placing a lens in the pump beam path before the dichroic mirror, there will be heating of the gold nanoparticle throughout the scan area. Which means that now the resolution will not be determined by the size of the pump beam but should be dictated by the thermal radius.

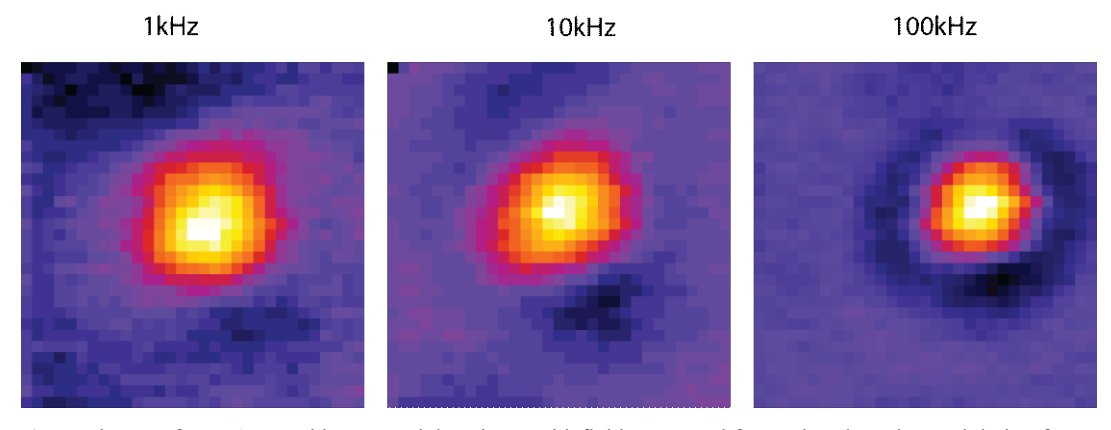


Figure 2. PHI images for a 50nm gold nanoparticle using a widefield pump and focused probe. The modulation frequency is shown at the top. The scan area was 3x3 µm with a step size of 100 nm and the time constant was 1s for every frequency.

The first thing to note is that much higher time constants are needed for the widefield scans. This is because the pump power density becomes much lower for a wider beam. Figure 2 shows that broadening is achieved as the frequency is lowered while using a widefield pump. Although, the full-width-half-maximum values for a line profile though the center of the particle are still smaller than the values predicted by R_{th} . Again, at 1 kHz the R_{th} is predicted to be 5.2 μ m, while the resolution achieved was much smaller. In order to better understand the frequency dependence for the spatial resolution, finite element simulations were used to look at the heat decay from gold nanoparticles.

Since we do not model how the beam is interacting with the thermal lens in COMSOL, we use COMSOL to look at the temperature profile of the gold nanoparticle and make conclusions based on that. The first set of simulations were performed using a 10 kHz and 1 MHz square wave heating of the gold nanoparticle in a glycerol environment. By both observing how well the gold particle is following the square wave heating and looking at the temperature profile across the whole simulation region, we can gain an understanding of the frequency effect.

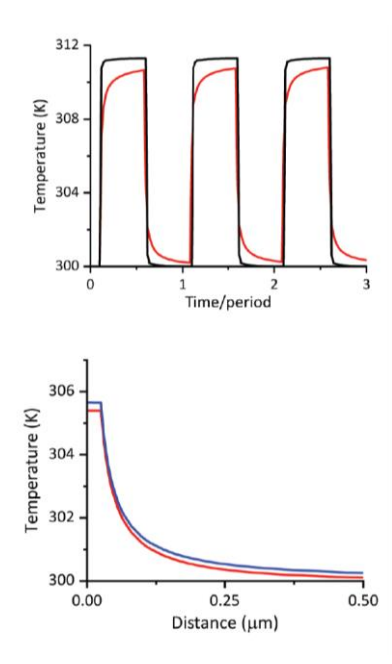


Figure 3. Simulated results for a 50nm gold nanoparticle in glycerol using a square wave heat source of 10 kHz (black) and 1 MHz (red). Top) Temperature vs normalized time (time/period) and bottom) Temperature vs distance profiles averaged over the three periods of heating.

The first thing we noticed was that for the temperature versus time traces, there is a significant difference between the two frequencies. At 10 kHz we can clearly see that the particle reaches steady state, where the rate of heating is equal to the rate of heat dissipation and the temperature is constant. On the other hand at high frequencies, there is not enough time for the particle to dissipate all of the heat between heating cycles, so the particle no longer is in steady state. In addition, the temperature vs distance profile at 10 kHz follows a 1/r decay, which is expected for steady state temperature conditions. On the other hand, high frequencies do not exactly follow the 1/r decay, which can be seen by comparing it to the 10 kHz decay. It is interesting to note that based on the time profile a larger effect for higher frequencies was predicted than what was observed in the distance profiles. In order to turn the temperature vs distance profiles into something tangible for the experiment, we took the full-width-quarter-maximum value from the temperature vs distance profiles to observe whether or not there is a frequency dependence in spatial resolution. The results for the different widths at different frequencies can be seen in figure 4.

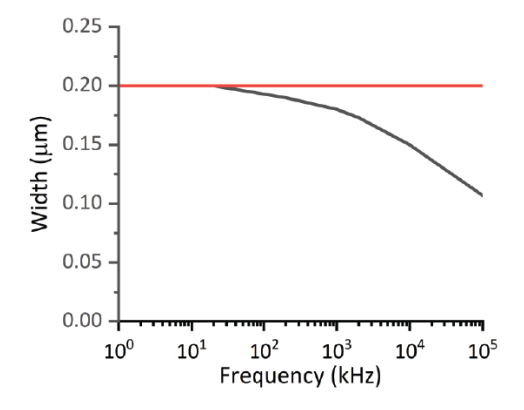


Figure 4. Full-width-quarter-maximum of the temperature profile for 50nm gold nanoparticles in glycerol. The red line shows the steady state solution.

The steady state solution is proportional to 1/r, 12 so the full-width-quarter-maximum is found when r is equal to 2*4*radius, or in this case $0.2 \mu m$. Note the extra factor of 2 is needed to determine the full width. What we found was

that for frequencies under about 50 kHz, the particle is in steady state conditions, and therefore the temperature decays away from the particle as 1/r. Hence at low enough frequencies, there is no longer any frequency dependence for the temperature profiles. On the other hand, at sufficiently high frequencies (> 50 kHz), for a 50 nm gold nanoparticle in glycerol there is a frequency dependence on the temperature profile. From the simulations, we can expect that there should be small changes in the PHI spatial resolution while going from high frequencies to low frequencies. Although these small differences could be hard to resolve due to the fact that the probe beam is convoluted with the temperature profile to create the PHI point-spread-function.

4. CONCLUSIONS

The effect of heat dissipation on the spatial resolution in PHI was investigated experimentally and through finite element simulations. There was no dependence on frequency found for gold nanoparticles imaged with a co-focused pump and probe. This is due to the fact that the PHI signal will only be created when the pump beam is actively heating the sample. For a widefield pump and focused probe it was found that there is a small frequency dependence on the spatial resolution. The spatial profile of the PHI signal in the widefield experiments still did not obtain the scale that was predicted by the thermal radius. Simulations showed that under 50 kHz frequency there should be no spatial resolution change since the particles reach a steady state where the temperature decays as 1/r from the particle. On the other hand for higher frequencies there can be a frequency dependence on the temperature profile and, therefore, the PHI point-spread-function.

ACKNOWLEDGEMENTS

The authors acknowledge the support of the National Science Foundation through Award CHE-1902403, and through a DOE SBIR Phase IIb grant. Any opinions, findings, and conclusions or recommendations expressed in this material are those of the authors and do not necessarily reflect the views of the National Science Foundation or the Department of Energy.

REFERENCES

- [1] Boyer, D.; Tamarat, P.; Maali, A.; Lounis, B.; Orrit, M., "Photothermal Imaging of Nanometer-Sized Metal Particles Among Scatterers," Science 297, 1160-1163, (2002).
- [2] Berciaud, S.; Cognet, L.; Blab, G. A.; Lounis, B., "Photothermal Heterodyne Imaging of Individual Nonfluorescent Nanoclusters and Nanocrystals," Phys. Rev. Lett. 93, 257402, (2004).
- [3] Adhikari, S.; Spaeth, P.; Kar, A.; Baaske, M. D.; Khatua, S.; Orrit, M., "Photothermal Microscopy: Imaging the Optical Absorption of Single Nanoparticles and Single Molecules," Acs Nano 14, 16414-16445, (2020).
- [4] Gaiduk, A.; Yorulmaz, M.; Ruijgrok, P. V.; Orrit, M., "Room-Temperature Detection of a Single Molecules Absorption by Photothermal Contrast," Science 330, 353-356, (2010).
- [5] Zhang, D.; Li, C.; Zhang, C.; Slipchenko, M. N.; Eakins, G.; Cheng, J.-X., "Depth-resolved mid-infrared photothermal imaging of living cells and organisms with submicrometer spatial resolution," Science Advances 2, e1600521, (2016).
- [6] Li, Z.; Aleshire, K.; Kuno, M.; Hartland, G. V., "Super-Resolution Far-Field Infrared Imaging by Photothermal Heterodyne Imaging," J. Phys. Chem. B 121, 8838-8846, (2017).
- [7] Berciaud, S.; Lasne, D.; Blab, G. A.; Cognet, L.; Lounis, B., "Photothermal heterodyne imaging of individual metallic nanoparticles: Theory versus experiment," Physical Review B 73, 045424, (2006).
- [8] Selmke, M.; Braun, M.; Cichos, F., "Photothermal Single-Particle Microscopy: Detection of a Nanolens," Acs Nano 6, 2741-2749.000, (2012).
- [9] Bhattacharjee, U.; West, C. A.; Hosseini Jebeli, S. A.; Goldwyn, H. J.; Kong, X.-T.; Hu, Z.; Beutler, E. K.; Chang, W.-S.; Willets, K. A.; Link, S.; Masiello, D. J., "Active Far-Field Control of the Thermal Near-Field via Plasmon Hybridization," Acs Nano 13, 9655-9663, (2019).
- [10] Gaiduk, A.; Ruijgrok, P. V.; Yorulmaz, M.; Orrit, M., "Detection limits in photothermal microscopy," Chemical Science 1, 343-350, (2010).
- [11] Pavlovetc, I. M.; Podshivaylov, E. A.; Chatterjee, R.; Hartland, G. V.; Frantsuzov, P. A.; Kuno, M., "Infrared photothermal heterodyne imaging: Contrast mechanism and detection limits," J. Appl. Phys. 127, 165101, (2020).
- [12] Carslaw, H. S.; Jaeger, J. C., [Conduction of Heat in Solids], Oxford University Press: Oxford, 261-263, (1959).